

Advances in Geosciences  
Vol. 12: Ocean Science (2007)  
Eds. Jianping Gan *et al.*  
© World Scientific Publishing Company

## IDENTIFICATION OF SPATIAL VARIABILITY AND EDDIES IN THE CIRCULATION OF THE SOUTH CHINA SEA

JIANPING GAN and HO SAN HO

*Department of Mathematics and the Atmospheric Marine and  
Coastal Environment Program, Hong Kong University of Science and  
Technology, Kowloon, Hong Kong, China*

A method of using a velocity Jacobian ( $J(u, v)$ ) to identify the spatial variability of the two-dimensional flow field has been delineated in detail. Positive and negative  $J(u, v)$  distinguish the vorticity-dominated and strain-dominated flows embedded in the mean general circulation, respectively. Normalized by the divergence of velocity, the non-dimensional  $J(u, v)$  becomes insensitive to the magnitude of the flow, illustrating the contrast between the strain- and vorticity-dominated flows. An index obtained from tracking the rotating angle of the fluid in a given point is employed to locate the eddy centers, saddle, and non-stationary points in the flow field. Both  $J(u, v)$  and the index are applied to the seasonal geostrophic circulation field in the South China Sea (SCS). They capture well the spatial flow variability and eddy centers or saddle points. Strong spatially variable flow fields, with alternating vorticity- and strain-dominated flows, are found in the basin scale flow along the continental margin. The index method, with a threshold of selected  $J(u, v)$ , clearly pinpoints seasonal eddies embedded in the mean circulation associated with the distinct regional forcing in the southwest and northeast SCS.

### 1. Introduction

Eddies are ocean currents that rotate as closed loops. They are embedded in the majority of low frequency oceanic currents. Eddies play an important part in modulating oceanic transport of heat and mass.<sup>24</sup> Eddies with amplitudes of 5–25 cm and diameters of 100–200 km contribute more than 50% of the variability over much of the world's oceans.<sup>2</sup> They are both the source and sink of variability in ocean circulation, particularly in regions with strong currents like western boundary currents, the Antarctic Circumpolar Current, and in the equatorial region. Eddies usually range in size from 50 to 200 km in diameter and elicit an increase in organisms

that comprise the marine food web. The swirling motion of eddies causes nutrients that are normally found in colder, deeper waters to come to the euphotic layer. The upwelling in eddies provides replenishment of nutrients that were depleted in the near-surface waters. The upwelling also substantially increases chlorophyll and plankton production.<sup>16,17</sup>

The intensity of an oceanic eddy is often measured by its vorticity or its angular velocity. However, an eddy does not necessarily have high vorticity; for example, a shear stream can have large vorticity but no eddy formation. A vortex can exist for a long time with concentrated vorticity; this is called a coherent structure. The formation of eddies can be described as the enstrophy (squared vorticity) that is being transferred from larger scale to smaller scale. This involves the transfer, coupling, and evolution of strain and vorticity in a turbulent flow. Many criteria were formulated for identifying the topology of coherent structures based either on arguments “concerned more with the evolution of material fluid tracers” (streak lines) or on arguments “concerned more with the appearance of fluid vectors (streamlines) and their comparison.” The Okubo–Weiss criterion uses the Okubo–Weiss parameter ( $W$ ) or velocity Jacobian,  $J(u, v)$ , to divide flow into strain-dominated and vorticity-dominated regions.<sup>19,27</sup> ( $u, v$ ) is the two-dimensional velocity field,  $V$ . It is based on the evolution of turbulent structures resulting from the analysis of the velocity gradient tensor,  $\nabla V$ . The  $Q$ -criterion,<sup>9</sup> combines the second invariant of  $\nabla V$ , i.e.,  $Q$  with pressure and velocity to characterize the streamlines into eddy zone, convergence zone, shear zone, and stream zone. The  $\lambda_2$ -criterion<sup>13</sup> further improves the  $Q$ -criterion by taking out the two-dimensional information of the plane associated with the three-dimensional flow. The  $\Delta$ -criterion<sup>1</sup> looks for the complex roots of  $\nabla V$  to detect the rotation of the streamlines, i.e., a vortex. These approaches all reduce to the  $Q$ -method under the assumption of two-dimensional incompressible flow. This method is based on the assumption of slowly varying flow or instantaneous flow. The problem becomes more transparent after adopting the reference axis of strain eigenvectors, the  $Q_s$  method, in two-dimensional flow which may be treated as a modification of the above criteria.<sup>24</sup> We regard the  $Q$  method as having “more geometry”, and the  $Q_s$  method as having “more dynamics” so that they mutually assist in the analyses instead of counteracting each other. Chakraborty *et al.*<sup>3</sup> suggested another Eulerian method which makes use of the real and imaginary parts of  $\nabla V$  to redefine an eddy. Haller<sup>8</sup> established the Lagrangian versions of  $Q$  and  $Q_s$ . He also developed a corresponding finite-time mixing enhancement and suppression in his two

separate studies. We have the time-independent approach, with snapshots of streamline geometry: the  $Q$  method, and a time-dependent approach with evolution of material line and surface: the  $Q_s$  method. Neither are equivalent, in general, but both may be re-expressed in a Lagrangian format. The former concerns the type of material shape formed, whereas the latter concerns the type of change of material shape. Haller<sup>9</sup> also established the  $M_z$  method, which is a generalization of the  $Q_s$  method for any three-dimensional flow in the sense of objective measurement on material lines and surfaces.

The  $Q$  method has been applied in oceanography to detect eddies. Isern-Fontanet *et al.*<sup>12–14</sup> discussed the utilization of  $Q$  (or Okubo–Weiss parameter, hereafter referred to as  $J(u, v)$ ) with a threshold  $Q = 0.2\sigma_Q$  to systematically identify marine eddies in the Algerian Basin and Mediterranean Sea from sea level anomaly (SLA) maps, where  $\sigma_Q$  is the spatial standard deviation of  $J(u, v)$ . The regions identified with high  $J(u, v)$  values were then separated into cyclonic and anti-cyclonic eddies according to the sign of the vorticity. Morrow *et al.*<sup>16</sup> adopted the method together with a SLA threshold to trace the different propagation directions of intensified cyclonic and anti-cyclonic vortices. The method was recently adopted by Chelton *et al.*<sup>2</sup> and by Henson and Thomas<sup>7</sup> to identify eddies in the global ocean and in the Gulf of Alaska, respectively.

The identification method cannot be simply reduced to a single  $Q$  method without the assumption of horizontal non-divergence. In general,  $J(u, v)$  can be linked with vorticity, strain, and divergence. The geometry of streamline snapshots can be theoretically divided into elliptic, parabolic, and hyperbolic regions.<sup>20</sup> In the limit of horizontal non-divergence inside the two-dimensional ocean flow, however, the assumption can be justified by the non-dimensional form of  $J(u, v)$  reflecting only elliptic and hyperbolic regions. The underlying assumption of horizontal non-divergence will be examined by normalizing  $J(u, v)$  over the domain.

The primary goal of this study is to present a methodology for identifying eddies and highly related spatially variable circulation structures from a given two-dimensional velocity field in the South China Sea (SCS). Considerable flow variability and eddies with different horizontal scales (Fig. 1) are embedded in the SCS basin-scale circulation as a result of interaction among the monsoon-driven current, remote current intrusion (e.g., Kuroshio) and the local topography.<sup>5</sup> From altimeter data, Wang *et al.*<sup>27</sup> found a great number of eddies in the SCS and grouped them into four eddy-active zones according to where they originated: southwest of

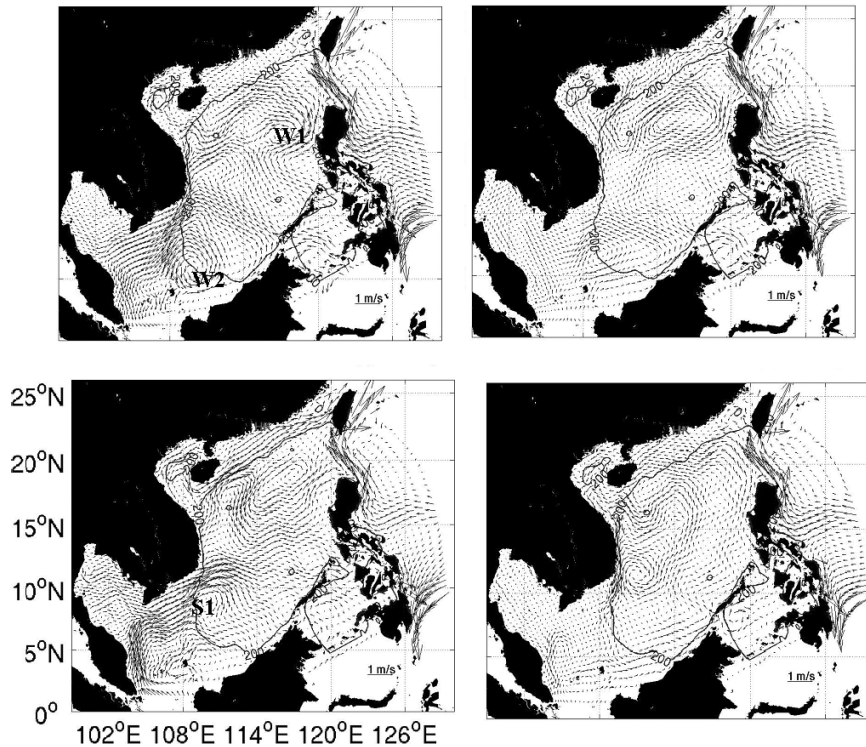


Fig. 1. The three-year (July 2000–June 2003) mean seasonal surface velocity vectors ( $\text{ms}^{-1}$ ) from a three-dimensional model. Major eddies embedded in the circulation are also marked. (Adopted from Ref. 5.)

Taiwan, northwest of the Luzon Strait, southwest of the Luzon Strait, and off central Vietnam. Various mechanisms for eddy formation are associated with the intrinsic dynamics in the respective zones as a result of interacting monsoon-inflow-topography. While it is not the objective of this study to investigate the formation mechanisms of the eddies, the mechanisms can be summarized to include: eddy-shedding by unstable fronts<sup>25,28</sup> and by Kuroshio intrusion dynamics<sup>31</sup> in the zone southwest of Taiwan (Fig. 1); land topography-induced wind stress curls in the zone northwest of the Luzon Strait (W1 in Fig. 1)<sup>22</sup> and, in the zone off central Vietnam<sup>30</sup> (S1); and coastal jet separation in the southwestern part of the SCS<sup>6</sup> (S1 and W2). Hwang and Chen,<sup>10</sup> based on analyses of altimetry data, identified the existence of warm-core and cold-core eddies in a widespread region of the SCS. Chu *et al.*<sup>4</sup> found that eddies in the northern and central SCS are

largely induced by the wind-stress curl. It is conceivable that eddies are also the source for creating spatial variability of the flow field in ambient waters. Gan and Qu<sup>6</sup> found that the anticyclonic/cyclonic eddy formations, owing to the summer/winter coastal current separation, characterize the structure of circulation and flow variability in the southwestern SCS.

## 2. Methods and Data

We will briefly clarify the geometric meaning of  $J(u, v)$  ( $Q$  method) and suggest a non-dimensional  $J(u, v)$ . We finally suggest a single quantity “index” which carries the topological property of  $J(u, v)$ , to achieve eddy identification.

### 2.1. Topological description

Eddies can be identified by the closed contours of SLA provided by altimetry data from satellite remote sensing. The contours determine local maximum/minimum of SLA. The geostrophic approximation is taken at the surface:

$$\begin{aligned}\frac{\partial h}{\partial x} &= -\frac{f}{g}v, \\ \frac{\partial h}{\partial y} &= \frac{f}{g}u,\end{aligned}\tag{1}$$

where  $h$  is the SLA and is equivalent to the stream function of surface geostrophic flow. A SLA extreme is equivalent to  $(u, v) = 0$  and  $J(u, v) > 0$  and can be used to identify a vorticity-dominated region with a stationary point (Appendix A). With the help of  $J(u, v)$ , one can extend the size of an enclosed circular eddy region to approximately its maximum velocity, where a change from convex to concave, or vice versa, takes place in the SLA.

Using  $J(u, v)$  alone, since  $(u, v) = 0$  cannot be ensured, one will identify not only the “vortex-region” with an eddy center, but also some “eddy-like-regions” possessing high vorticity without an eddy center; that is, the SLA isolines are not a closed loop. The “eddy-like-regions” can be interpreted as perturbations embedded in the background flow, or a fraction of an eddy without a center. One may further use a threshold, e.g.,  $J(u, v) > \text{threshold}$ , to systematically separate these two types of regions and to obtain the intensified “vortex-regions” with the added cost of filtering some eddies.<sup>10</sup>

The strain-dominated region embedded in  $J(u, v)$  represents the spatial structure of the flow field which is an important component for characterizing the overall flow structure. The stationary points possessing significant strain value are ignored after using the criteria maximum/minimum of SLA. Although the strain-dominated region can still be identified by indefinite type in the SLA, it is more convenient to use the relation:  $J(u, v) < 0$ .

## 2.2. Geometry of $J(u, v)$ (or $Q$ method)

From the geometric argument in Appendices A and B,  $J(u, v)$  can be interpreted as the tendency of ellipticity (eddy), parabolicity (node), or hyperbolicity (saddle) of the flow field embedded in a uniform flow for three-dimensional (Appendix A) and two-dimensional (Appendix B) flows. It can be physically interpreted as the combination of divergence, rotation, and strain. In incompressible flow, it is mainly the competition between rotation and strain. Detailed derivations for both three-dimensional and two-dimensional flows are presented in Appendices A and B.

In this study, we will use two-dimensional flow  $(u, v)$  to investigate eddies and the flow field in the SCS.  $J(u, v)$  of a two-dimensional flow has the following form and decomposition:

$$\begin{aligned}
 J(u, v) &= u_x v_y - u_y v_x \\
 &= \underbrace{\left(\frac{v_x - u_y}{2}\right)^2}_{\text{rotation magnitude}^2} - \underbrace{\left(\left(\frac{v_x + u_y}{2}\right)^2 + \left(\frac{u_x - v_y}{2}\right)^2\right)}_{\text{strain magnitude}^2} \\
 &\quad + \underbrace{\left(\frac{u_x + v_y}{2}\right)^2}_{\text{divergence magnitude}^2}. \tag{2}
 \end{aligned}$$

On the right-hand side of the equation, the first term can be interpreted as average rotation speed; the second term represents the magnitude of strain, and the last term, which is zero in non-divergent flow, is the average horizontal divergence. The positive value from the last term of horizontal divergence can be mixed with the positive vorticity in  $J(u, v)$  from the first term. Thus, an eddy center and a node point cannot be distinguished when

divergence is not negligible and  $J(u, v)$  takes a positive value. We propose a non-dimensional form,

$$N_2 = \frac{J(u, v)}{\left[\frac{u_x + v_y}{2}\right]^2} \quad (\text{Appendix B}), \quad (3)$$

which directly checks the significance of the horizontal divergence over the whole domain at once. A small value of horizontal divergence amplifies  $J(u, v)$  “close to infinity”, and leaves the “divergence region with significant upward motion” staying between zero and one. Thus, the divergence effect can be neglected if  $N_2 \gg 1$  or  $\ll 0$ , then the value is simply reflecting the sign of  $J(u, v)$ . A similar analysis can be carried out on three-dimensional flow (Appendix A).

### 2.3. Index and sector

We propose a simple topological quantity, an “index”, to identify eddy centers: the rotating angle of a point with respect to a vector field. We call it a “rotated angle” to retain its intuitive meaning. Using this criterion provides a more systematic way of identifying eddies than visual inspection of SLA extrema. The index recognizes eddy centers without considering the strength of velocity so one can filter the result within a certain range of  $J(u, v)$  strength. The method can be used to track eddy movements; for instance, to study the mingling and scattering among eddies which are close to each other.

The index of a point is defined as the rotating angle per  $2\pi$ . The rotating angle is the change in angle when one is traveling along a sufficiently small loop around a point following the direction of the vector field. It is clearly independent of the initial position because it can be written as this infinitesimal integral:  $\delta\theta = \oint d(\tan^{-1} \frac{v}{u})$ . It is a multiple of  $2\pi$  because a vector can rotate integer number of times around the closed loop back to its initial location under the condition that every stationary point can be isolated by a sufficiently small loop in a continuous linearized flow. We conclude with the assumption (Fig. 2):

$$\text{index} = \begin{cases} 0, & \text{not a stationary point,} \\ 1, & \text{eddy center or node point,} \\ -1, & \text{saddle point.} \end{cases}$$

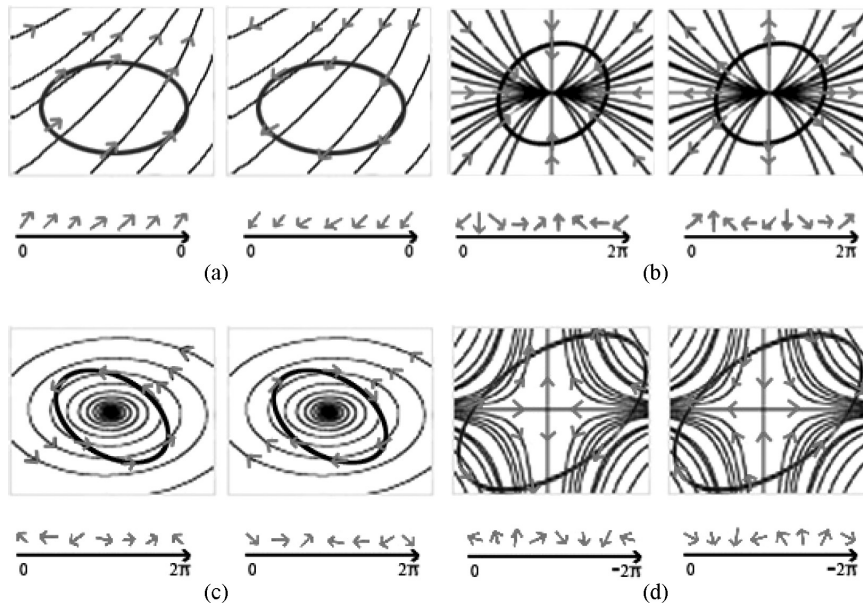


Fig. 2. Rotating angle of a loop. The rotated angle is zero around (a) a non-singular point; (b) a node point; (c) the angle has a value  $2\pi$  in the eddy's center; and (d) a saddle point has a value  $-2\pi$ .

The index (rotating angle) is a topological counterpart to  $J(u, v)$ . The index and  $J(u, v)$  take the same sign for every linearized point. It can be directly checked that the rotating angle is  $-2\pi$  for a saddle point and  $2\pi$  for an eddy center, or, equivalently, index =  $-1$  for a saddle point, and 1 for an eddy center. In the absence of horizontal divergence, there is no node point ( $1 > N_2 > 0$ ) as demonstrated in Appendix B and a stationary point can be a saddle point or an eddy center.

### 3. Applications

#### 3.1. Data

To identify the seasonal nature of eddies and the associated spatial variability in the flow field we calculate the seasonal  $J(u, v)$ ,  $N_2$ , index with threshold  $J(u, v)$  in the SCS from the mean surface geostrophic currents averaged over 3 years from July 1, 2000 to June 20, 2003. The surface geostrophic currents are produced by the Archiving, Validation,

and Interpolation of Satellite Oceanographic Data (AVISO) project in France. The data are archived into a grid of  $1/3^\circ$  resolution and in fractions of a week temporally. The geostrophic currents were calculated from the absolute dynamic topography consisting of the anomalies of the altimeter sea level and a Mean Dynamic Topography (MDT). The MDT was computed with different types of data including altimetry, *in situ* measurements, and a geoid model. The method of estimating the MDT is explained in detail by Rio and Hernandez.<sup>23</sup> Over the shelf area, however, the data still contain aliases from tides and internal waves. Thus, the data over the shelf, shallower than 200 m, are masked.

### 3.2. Seasonal $J(u,v)$

The seasonal mean of surface geostrophic velocity vectors and  $J(u,v)$  (Fig. 3) exhibit a strong variable flow field in the SCS in all seasons. With the dominant currents are along quasi-horizontal density surface, the divergence in geostrophic currents can be neglected. Thus, positive and negative  $J(u,v)$  represent the vorticity- and strain-dominated flows, respectively. In general, vorticity- and strain-active region alternate spatially. Water with a strong positive  $D_2$  or  $J(u,v)$  is generally accompanied with a corresponding strong negative  $D_2$ . Vorticity-active or strain-active flows occur primarily along the continental margin associated with the interaction of the dominant basin-scale circulation with slope topography. In the western part of the Luzon Strait the active flows are a result of Kuroshio intrusion. To the east of Vietnam and to the west of the central Luzon Islands they are produced by topography-induced wind stress curls. A vorticity/strain active region is also found in the central part of the basin, particularly in the fall. These eddies seem to originate at the western boundary off central Vietnam because of the confluence of southward and northward currents as monsoons shift from southerly to northeasterly.<sup>5</sup>

The vorticity-dominated flow may form oceanic eddies although they cannot be identified by  $J(u,v)$  alone. As shown in the vector field, strong eddies with spatially variable flow fields exist in the regions to the southeast and to the east off central Vietnam in the winter and summer, respectively. The energetic eddies are formed by the combined forces of wind stress curls and coastal jet separation.<sup>6</sup>

As the non-dimensional value of  $D_2$  (Appendix B),  $N_2$  is not sensitive to the magnitude of the flow and is able to illustrate the contrasting flow field. Because  $N_2$  is non-dimensional, its field simply reflects the flow

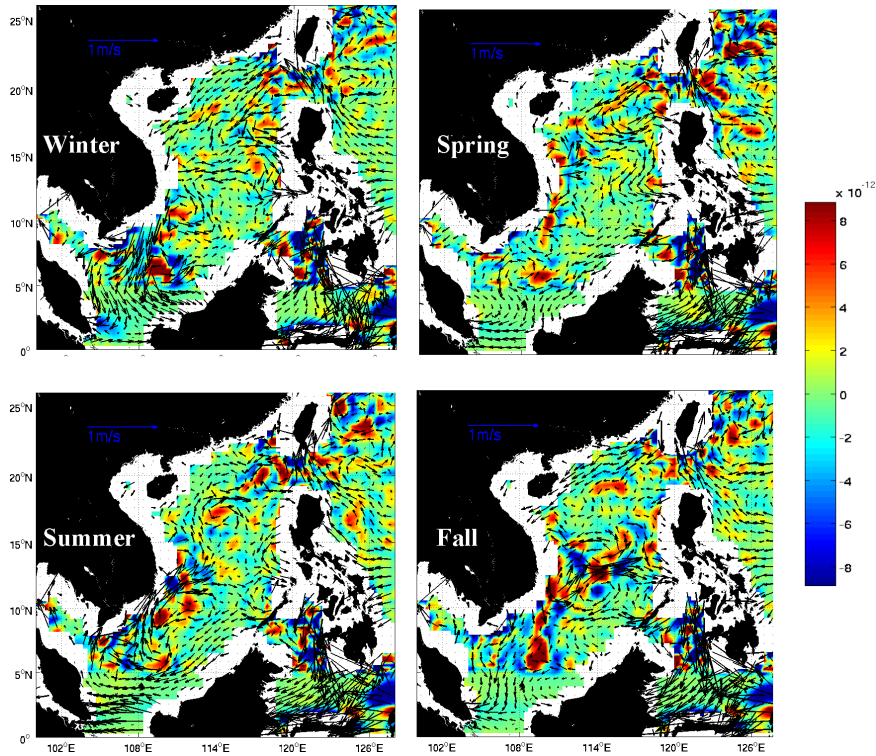


Fig. 3. The three-year average of seasonal distribution of the surface geostrophic velocity Jacobian  $D_2 = J(u, v)$ . Positive and negative  $D_2$  represent the vorticity- and strain-dominated flows, respectively.

direction as either vorticity- or strain-dominated. Figure 4 indicates the nature of alternating distributed vorticity-strain flows in the circulation of SCS. Among them, the distinctly vorticity-dominated summer flows are found in the southwest SCS. Although the value of  $J(u, v)$  is generally smaller in the central part of the basin,  $N_2$  suggests that the flows are still highly variable in space.

### 3.3. Eddy center identification

The eddy centers and the saddle points identified by the index are presented in Fig. 5 for the surface geostrophic currents in the winter and summer. One can detect from their vector counterparts that the index realistically locates

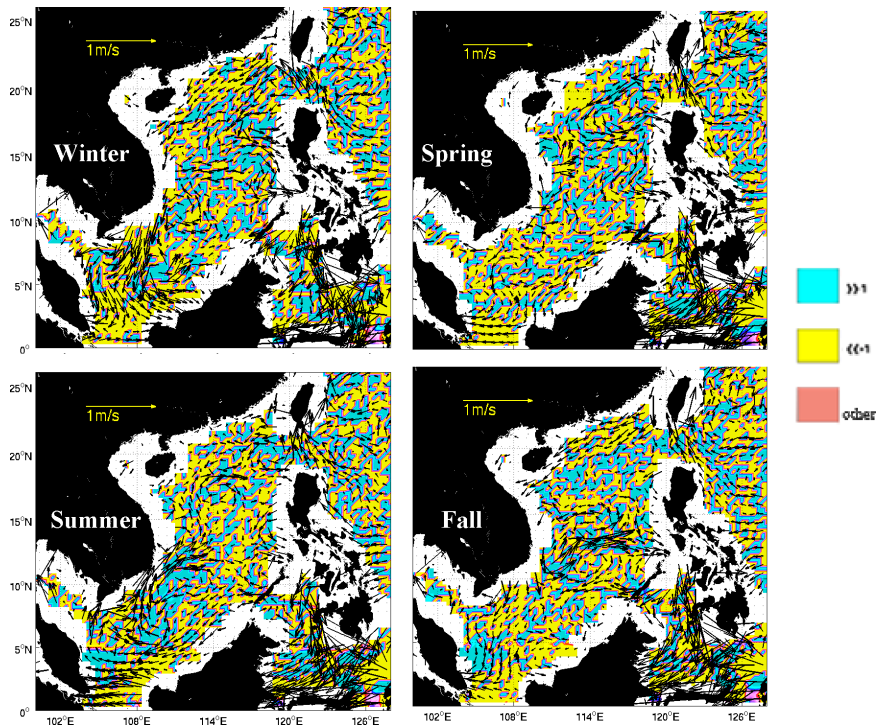


Fig. 4. The three-year average of seasonal distribution of  $J(u, v)$  in non-dimensional form,  $N_2$ .

the stationary points either as eddy centers or as saddle points. At the same time  $J(u, v)$  is able to distinguish the region of vorticity-dominated regions from strain-dominated regions and the index can pick out the centers of the eddies and saddle points. Because  $J(u, v)$  cannot distinguish an eddy in a vorticity-dominated region and the index cannot differentiate the weak eddies from those strong ones, we combined the index and  $J(u, v)$  with a threshold to better identify dominant eddies. The threshold for  $J(u, v)$  can be subjectively selected to show the best filtering effect. With a value of  $6 \times 10^{-12} \text{ s}^{-2}$ , energetic eddies associated with seasonal characteristics of basin-scale circulation are identifiable (Fig. 6). Although it requires additional information like signs of either vorticity or SLA to distinguish cyclonic from anticyclonic eddies, Fig. 6 clearly shows the characterized cyclonic eddies in the southwest of the SCS and west of the Luzon Islands in the winter as well as the anticyclonic eddy to the east of central Vietnam and the cyclonic eddy west of the Luzon Strait in the summer.

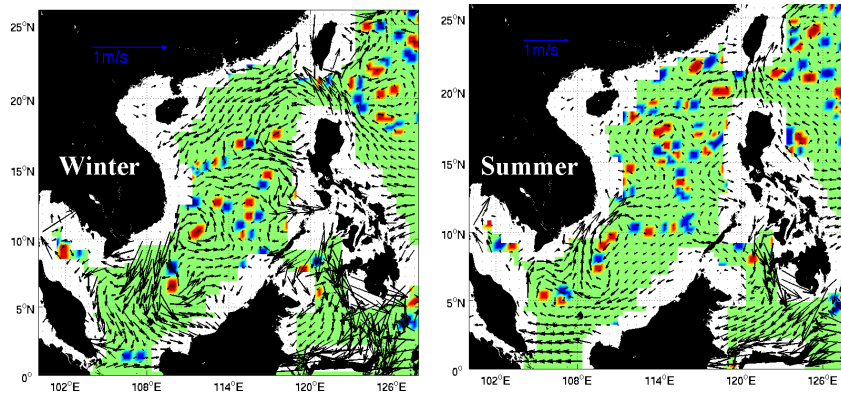


Fig. 5. Surface geostrophic velocity vectors and rotated angle ( $= \oint d\theta$ ). Red ( $= 2\pi$ ) indicates the center of an eddy and blue ( $= -2\pi$ ) indicates a saddle point.

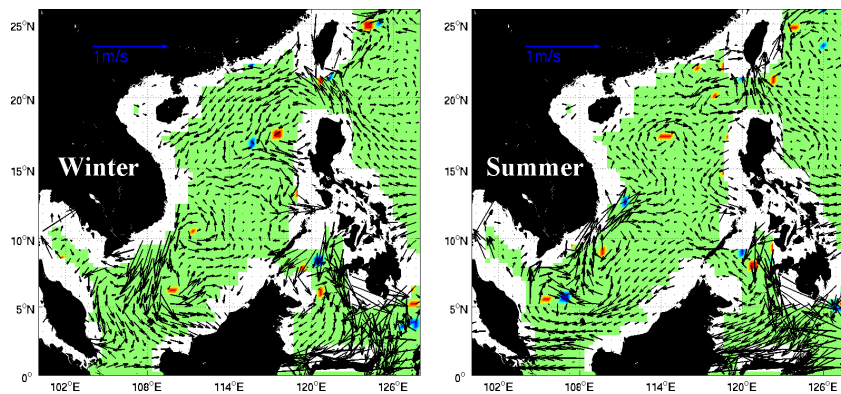


Fig. 6. As in Fig. 5 but only those values with  $J(u, v) \geq 6 \times 10^{-12} \text{ s}^{-2}$  are shown.

#### 4. Summary

We have described a method for identifying eddy centers that is based on a velocity Jacobian and an index that tracks the rotating angle of the fluid in a given point in a spatially variable flow field. The Jacobian method alone, or Okubo–Weiss parameter,<sup>19,27</sup> is able to find the vorticity-dominated and strain-dominated flows embedded in the mean general circulation. While the results obtained from Jacobian implicitly assume a non-divergent flow, the non-dimensional velocity Jacobian is insensitive to flow magnitude and illustrates the contrasting flow field. The index tracks the rotating angle of the fluid around a given point and locates the eddy centers, saddle points, and non-stationary points.

Using surface geostrophic currents derived by AVISO, the method was applied to the SCS to distinguish flow field variability and to identify eddies in different seasons. The results obtained from the method captured the seasonal variability in the surface geostrophic flow field very well. It was found that the highly variable seasonal flow field alternated between vorticity- and strain-dominated flows. Strong vorticity flow is generally accompanied with strong strain flow around it. Intensified vorticity-strain flow variability exists in the continental margin along the track of the dominant circulation. A selection of thresholds for  $J(u, v)$  would allow us to scrutinize the major spatial variability in the flow field.

The index method, an alternative for identifying eddy centers, extracts eddies embedded in the mean circulation field. Combined with a threshold for selecting  $J(u, v)$ , eddies associated with distinct physical forcing in the southwest and northeast of SCS were pinpointed.

**Acknowledgment**

This research was supported by the Research Grants Council of Hong Kong under Grants CERG-601006 and N\_HKUST623/07.

**Appendix A. Three-Dimensional Local Linearized Differential Equation Streamline Solution**

With regard to the classification method of a singular point of a system of ordinary differential equations (ODE), one can decompose the field into a uniform field and a background field in the neighborhood of any point. That is, in a fixed time,  $t_0$ , we can carry out the Taylor expansion on  $u(x, y, t_0)$ ,  $v(x, y, t_0)$ , and  $w(x, y, t_0)$ , keeping first order terms to get the local linear approximation

velocity field	velocity at that point	background velocity for that point
-------------------	------------------------------	--

$$\begin{pmatrix} u \\ v \\ w \end{pmatrix} = \begin{pmatrix} u_0 \\ v_0 \\ w_0 \end{pmatrix} + \overbrace{\frac{\partial(u, v, w)}{\partial(x, y, z)} \begin{pmatrix} x - x_0 \\ y - y_0 \\ z - z_0 \end{pmatrix}} + o(x - x_0) + o(y - y_0) + o(z - z_0)$$

where  $\frac{\partial(u, v, w)}{\partial(x, y, z)}$  is the Jacobian matrix,  $\begin{pmatrix} u_x & u_y & u_z \\ v_x & v_y & v_z \\ w_x & w_y & w_z \end{pmatrix}_{x_0, y_0, z_0, t_0}$ .

In other words, locally, the field is decomposed into a uniform flow and a “background flow variation.”

We assume that the Jacobian determinant (i.e.,  $\det \frac{\partial(u,v,w)}{\partial(x,y,z)}$ ) is non-zero so that the background flow can be linearized. Thus, the information of the local linearized flow (until any non-singular transformation of expansion/contraction, shear, and rotation) is stored in the three coefficients ( $c^1$ ,  $c^2$ , and  $c^3$ ) of the characteristic equation

$$-\lambda^3 + c^1\lambda^2 - c^2\lambda + c^3 = 0, \quad (\text{A.1})$$

$$c^1 = \text{div}(\vec{v}),$$

$$c^2 = \det \frac{\partial(u,v)}{\partial(x,y)} + \det \frac{\partial(v,w)}{\partial(y,z)} + \det \frac{\partial(u,w)}{\partial(x,z)},$$

$$c^3 = \det \frac{\partial(u,v,w)}{\partial(x,y,z)},$$

where  $\lambda$  is an eigenvalue of the Jacobian matrix. In an incompressible oceanic flow, the coefficient  $c^1$  vanishes. Thus, the degrees of freedom of the flow field reduce to two which are provided by  $c^2$  and  $c^3$ . These two parameters can be combined to form a single parameter

$$D_3 = \left( \left( \det \frac{\partial(u,v)}{\partial(x,y)} + \det \frac{\partial(v,w)}{\partial(y,z)} + \det \frac{\partial(u,w)}{\partial(x,z)} \right) / 3 \right)^3 + \left( \det \frac{\partial(u,v,w)}{\partial(x,y,z)} / 2 \right)^2$$

or its non-dimensional form,

$$N_3 = \frac{\left( \left( \det \frac{\partial(u,v)}{\partial(x,y)} + \det \frac{\partial(v,w)}{\partial(y,z)} + \det \frac{\partial(u,w)}{\partial(x,z)} \right) / 3 \right)^3}{\left( \det \frac{\partial(u,v,w)}{\partial(x,y,z)} / 2 \right)^2},$$

which defines the characteristics of the streamline without flow direction in (A.1) when the fluid is incompressible. While the dimensional  $D_3$  is sensitive to the magnitude of the flow, the non-dimensional  $N_3$  is not.  $N_3$  can illustrate the contrasting flow field. Characterized types of three-dimensional background flow variations in term of  $D_3$  and  $N_3$  are displayed in Fig. A1.

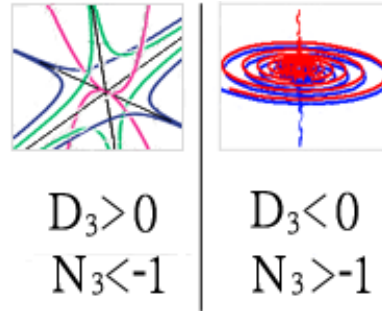


Fig. A1. Characterized types of three-dimensional background flow variation. The streamlines (red, blue, and green lines) in the left panel from the three eigenvectors (black lines) represent the node (red line) and saddle (blue and green lines) flow patterns. In the right panel,  $D_3 > 0$  or  $N_3 < -1$  represents a flow with two saddle planes and one node plane;  $D_3 < 0$  or  $N_3 > -1$  represents a spiraling vortex exponentially closing to (departing from) its center axis toward (away from) the top and bottom. The streamlines in the figure are up to a linear transformation.

### Appendix B. Two-Dimensional Local Linearized Differential Equation Streamline Solution

Since the magnitude of vertical velocity in the ocean is three to four orders of magnitude smaller than that of horizontal velocity, ocean flow is approximately two-dimensional. When one takes a cross-section or depth-average of a specific layer from a three-dimensional flow, the two-dimensional flow obtained will be, in general, compressible. Similarly, we can get the corresponding  $D_2 = \det \frac{\partial(u,v)}{\partial(x,y)}$  and its non-dimensional parameter,  $N_2 = \frac{\det \frac{\partial(u,v)}{\partial(x,y)}}{(u_x + v_y/2)^2}$ , from the two-dimensional characteristic equation

$$\lambda^2 - c1\lambda + c2 = 0, \quad (\text{B.1})$$

and

$$\begin{aligned} c1 &= \text{div}(\vec{v}), \\ c2 &= \det \frac{\partial(u,v)}{\partial(x,y)}. \end{aligned}$$

Here,  $x, y, u, v$  are the axes and velocity with respect to rectangular coordinates on the cross-sectional plane. It classifies a non-degenerating background flow variation as saddle, node, and vortex (Fig. B1).

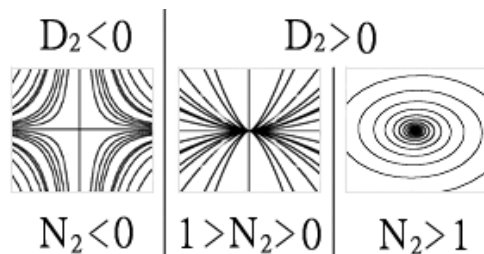


Fig. B1. Types of cross-sectional background flow variation. The left panel represents a plane with a saddle point; the middle represents a plane with a node point; and the right panel represents a plane with a spiral point.

Under the limits of an incompressibility condition,  $D_2 = \det \frac{\partial(u,v)}{\partial(x,y)}$  and  $N_2 = \text{sign}(\det \frac{\partial(u,v)}{\partial(x,y)})$ .  $D_2$  is known as the Jacobian of velocity, and is usually denoted by  $J(u,v)$ . Although  $D_3$  helps to understand the real three-dimensional structure of the flow, it is, however, hard to accurately calculate due to uncertainty in the vertical velocity in the ocean. In this study, the two-dimensional solution is used to identify the partially variable flow field and existing eddies.

## References

1. M. S. Chong, A. E. Perry and B. Cantwell, A general classification of three-dimensional flow field, *Phys. Fluids* **12** (1990) 2478–2488.
2. D. B. Chelton, M. G. Schlax, R. M. Samelson and R. A. de Szoeke, Global observations of large oceanic eddies, *Geophys. Res. Lett.* **34** (2007) L15606.
3. Adrian, On the relationships between local vortex identification schemes, *J. Fluid Mech.* **535** (2005) 189–214.
4. P. Chu and C. Fan, Low salinity, cool-core cyclonic eddy detected northwest of Luzon during the South China Sea Monsoon Experiment (SCSMEX) in July 1998, *J. Oceanogr.* **57** (2001) 549–563.
5. J. P. Gan, H. Li, E. N. Curchitser and D. B. Haidvogel, Modeling South China Sea circulation: Response to seasonal forcing regimes, *J. Geophys. Res.* **111** (2006) C06034, doi: 10.1029/2005JC003298.
6. J. P. Gan and T. D. Qu, Coastal jet separation and associated flow variability in the southwest South China Sea, *Deep-Sea Res. I* **55** (2008) 1–19.
7. S. A. Henson and A. C. Thomas, A census of oceanic anticyclonic eddies in the Gulf of Alaska, *Deep-Sea Res. I* **66** (2008) 163–176.
8. G. Haller, Lagrangian structures and the rate of strain in a partition of two-dimensional turbulence, *Phys. of Fluids*, **13** (2001) 11.
9. G. Haller, An objective definition of a vortex, *J. Fluid Mech.* **525** (2005) 1–26.

10. C. Hwang and S. A. Chen, Circulations and eddies over the South China Sea derived from TOPEX/Poseidon altimetry, *J. Geophys. Res.* **105** (2000) 23943–23965.
11. J. Hunt, A. Wray and P. Moin, Eddies, stream, and convergence zones in turbulent flows, *Proc. CTR Summer Program*, Stanford, CA, Center for Turbulence Research, 1988, pp. 193–208.
12. J. Isern-Fontanet, E. García-Ladona and J. Font, Identification of marine eddies from altimetric maps, *J. Atmos. Oceanic Technol.* **20** (2003) 772–778.
13. J. Isern-Fontanet, J. Font, E. García-Ladona, M. Emelianov, C., Millot, I. Taupier-Letage, Spatial structure of anticyclonic eddies in the Algerian Basin (Mediterranean Sea) analyzed using the Okubo–Weiss parameter, *Deep-Sea Res. II* **51** (2004) 3009–3028.
14. J. Isern-Fontanet, E. García-Ladona and J. Font, Vortices of the Mediterranean Sea: An altimetric perspective, *J. Phys. Oceanogr.* **36** (2006) 87–103.
15. J. Jeong and F. Hussain, On the identification of a vortex, *J. Fluid Mech.* **285** (1995) 69–94.
16. R. Morrow, F. Birol, D. Griffin and J. Sudre, Divergent pathways of cyclonic and anti-cyclonic ocean eddies, *Geophys. Res. Lett.* **31** (2004) L24311, doi: 10.1029/2004GL020974.
17. V. M. Kamenkovich, M. N. Koshlyakov and A. S. Monin (eds.), *Synoptic Eddies in the Ocean* (D. Reidel, 1986), 433 pp.
18. A. P. Martin and K. J. Richards, Mechanisms for vertical nutrient transport within a North Atlantic mesoscale eddy, *Deep-Sea Res. I* **48** (2001) 757–773.
19. D. J. McGillicuddy, A. R. Robinson and J. J. McCarthy, Coupled physical and biological modeling of the spring bloom in the North Atlantic (II): Three dimensional bloom and post-bloom processes, *Deep-Sea Res. I* **42** (1995) 1359–1398.
20. J. C. McWilliams, The emergence of isolated, coherent vortices in turbulent flow, *J. Fluid Mech.* **42** (1984) 21–43.
21. A. Okubo, Horizontal dispersion of floatable particles in the vicinity of velocity singularities such as convergences, *Deep Sea Res.* **17** (1970) 445–454.
22. T. D. Qu, Upper-Layer circulation in the South China Sea, *J. Phys. Oceanogr.* **30** (2000) 1450–1460.
23. M.-H. Rio and F. Hernandez, A mean dynamic topography computed over the world ocean from altimetry, *in situ* measurements, and a geoid model, *J. Geophys. Res.* **109** (2004) C12032, doi: 10.1029/2003JC002226.
24. A. Robinson, *Eddies in Marine Science*, (Springer Verlag, 1983), 609 pp.
25. J. L. Su, J. P. Xu, S. Q. Cai and O. Wang, Gyres and eddies in the South China Sea, *in Onset and Evolution of the South China Sea Monsoon and Its Interaction with the Ocean*, eds. Y. Ding and C. Li (China Meteorological Press, 1999), pp. 272–279.
26. M. Tabor and I. Klapper, Stretching and alignment in chaotic and turbulent flows, *Chaos Soliton Fract.* **4** (1994) 1031–1055.
27. G. H. Wang, J. L. Su and P. C. Chu, Mesoscale eddies in the South China Sea observed with altimeter data, *Geophys. Res. Lett.* **30** (2003) 2121, doi: 10.1029/2003GL018532.

28. L. P. Wang, C. J. Koblinsky and S. Howden, Mesoscale variability in the South China Sea from the TOPEX/Poseidon altimetry data, *Deep-Sea Res. I* **47** (2000) 681–708.
29. J. Weiss, The dynamics of enstrophy transfer in two-dimensional hydrodynamics. *Physica D* **48** (1991) 273–294.
30. S. Xie, Q. Xie, D. Wang and W. T. Liu, Summer upwelling in the South China Sea and its role in regional climate variations, *J. Geophys. Res.*, **108** (2003) 3261, doi:10.1029/2003JC001867.
31. H. Xue, F. Chai, N. Pettigrew, D. Xu, M. Shi and J. Xu, Kuroshio intrusion and the circulation in the South China Sea, *J. Geophys. Res.* **109** (2004) C02017, doi: 10.1029/2002JC001724.